IEEE Access
Multidisciplinary | Rapid Review | Open Access Journal

Received November 28, 2018, accepted December 8, 2018, date of publication December 17, 2018,
date of current version January 7, 2019.

*Digital Object Identifier 10.1109/ACCESS.2018.2886644*

# Applying Bayesian Network Approach to Determine the Association Between Morphological Features Extracted from Prostate Cancer Images

**LAL HUSSAIN[1], AMJAD ALI[2,3], SAIMA RATHORE[4], SHARJIL SAEED[1], ADNAN IDRIS[5], MUHAMMAD USAMA USMAN[6], MUHAMMAD AKSAM IFTIKHAR[2], AND DOUG YOUNG SUH[3], (Member, IEEE)**

[1]Department of Computer Science and IT, University of Azad Jammu and Kashmir, Muzaffarabad 13100, Pakistan
[2]Department of Computer Science, COMSATS University Islamabad, Lahore 54000, Pakistan
[3]College of Electronics and Information, Kyung Hee University, Yongin 17140, South Korea
[4]Department of Radiology, University of Pennsylvania, Philadelphia, PA 19104, USA
[5]Department of Computer Science and IT, The University of Poonch Rawalakot, Rawalakot 12350, Pakistan
[6]Department of Electrical and Computer Engineering, Florida State University, Tallahassee, FL 32306, USA

Corresponding author: Doug Young Suh (suh@khu.ac.kr)

This work was supported by the MSIT (Ministry of Science and ICT), South Korea, through the Grand Information Technology Research Center support program supervised by the IITP (Institute for Information & communications Technology Promotion) under Grant IITP-2018-2015-0-00742.

**ABSTRACT** Cancer is a major public health problem across the globe due to which millions of deaths occur every year. In the United States, prostate cancer is the second leading cause of cancer- related deaths in men. The major causes of prostate cancer include increasing age, family history, diet, sexual behavior, and geographic location. Early detection of prostate cancer can effectively reduce the mortality rate. In the past, researchers have adopted various multimodal feature extracting strategies to extract diverse and comprehensive quantitative imaging features and employed machine learning methods to detect prostate cancer. However, existing techniques lack detailed analysis of the magnitude of relationship among different individual discriminatory features, which is very important to understand the dynamics of the disease. In this study, we extracted diverse morphological features to summarize the imaging profile of patients of prostate cancer imaging database and employed Bayesian network analysis approach to quantify the association between different features and the strength of the association. The features and the association between the features were, respectively, modeled as the nodes and the edges of the network. The strength of association between the nodes was computed using Pearson's correlation, mutual Information and Kullback–Liebler methods. The strongest associations were found between multiple features: (Area → Equidiameter), (Area → Circulatory 2), (Circulatory 1→ (Elongatedness), (Circulatory 1→ Entropy), (Circulatory 1→ Max. Radius), and (Min. Radius → Eccentricity). Moreover, interaction impact among nodes and node force was also computed. This analysis will help in finding the features that are more dominant to establish the relationship and can further increase the detection performance.

**INDEX TERMS** Bayesian network analysis, coherence, prostate cancer, morphological features, Pearson's correlation, mutual information, Kullback Liebler.

## I. INTRODUCTION

Prostate Cancer (PCa) is commonly diagnosed cancer (>200 per 100,000 men/year) in men [1] and remains the second leading cause of cancer-related deaths in men worldwide. The projected rate of prostate cancer-related deaths is estimated to be 164,690 (19%) world-wide and 29,430 (9%) in United States [2]. Approximately 609,640 deaths were expected due to colon cancer in American men in 2018 only.

The PCa is suggested to be the consequence of exogenous factors including chronic inflammation, diet, low exposure

to ultraviolet radiation and sexual behavior [3]. The family history of PCa (both maternal and paternal [4]), dietary factors, dairy products, body size, sexual behavior and sexually transmitted diseases, smoking, alcohol, and age, are the well-established risk factors. The risk increases 5-11 times when two or more blood-relatives are affected [5]. About 9% of men suffered from PCa have a truly genetic disease associated with an onset of 6-7 years earlier than the spontaneous cases.

Medical imaging has gained much importance in the last few decades to analyze the different body parts [6]. Different clinical diagnostic tools such as transrectal ultrasound (TRUS), digital rectal examination (DRE), prostate specific antigen (PSA) and biopsy tests are most widely used for detecting prostate cancer irrespective of acquiring accurate results [7]. PSA has been extensively used to detect PCa at an early stage. It is imperative to identify the new accurate biomarker that allows the early detection of PCa to distinguish aggressive between insignificant tumors. In 2001, about 75% of American men at the age of 50+ years have undergone PSA test at least once [8], whereas, the annual rates of PSA were lower in other countries such as Germany [9]. In USA, PSA testing is used to detect the PCa at earlier stage and has shifted the spectrum of diagnosed cancers towards an increased diagnosis of moderately differentiated tumors.

TRUS-Guided Biopsy (TRUS-GB) is another tool to evaluate the suspected PCa, however, it has several limitations: (i) having a low detection rate (27-40%), (ii) Gleason score underestimation (34-46%) compared to the Gleason score estimated in radical prostatectomy specimens, (iii) and relatively high detection of clinically insignificant cancers [10]– [12]. Another promising tool (Magnetic resonance imaging, MRI) is gaining importance to evaluate the PCa. The accuracy for detecting and localizing PCa is improved with the introduction of multiparametric MRI (mpMRI) [13]– [16]. The research also revealed that mpMRI-guided biopsy (MRGB) process has improved the quality of targeted biopsy [17], [18] resulting in high detection rate of PCa.

Medical image segmentation and analysis [19], [20] is done by employing different image processing techniques. Recently, [21] employed correlated regression features for automated segmentation of right ventricle (RV) which can tackle complex variable crescent shape, local weak/no boundary inhomogeneous intensity of RV simultaneously. This method combines holistic regression model with convolution neural network (CNN) to determine the RV boundary points simultaneously and directly for which in the past researchers applied many effective methods for RV segmentation from cardiac images [22]– [28]. Likewise, [29] employed Deep temporal regression networks to detect and recognize end-diastole and end systole frames from cine MRI to evaluate cardiovascular functions by integrating convolution neural network (CNN) with recurrent neural network (RNN). The CNN from Deep learning has been most widely used approaches for analysis of medical images [30]– [32].

The Bayesian networks (BNs) have been used to develop relationship among genes, environment and diseases [33], gene-environmental factors [33], medical diagnosis, forensic science, crime and terrorism risk, and ecological conservation [33], analyzing gene expression data [34], [35], predict protein-protein interactions [36], derive protein signalling networks [37]– [39], perform pedigree analysis [36], and to assess the performance of microsatellite markers on cancer recurrence [40].

Recently, [41] applied spatially structured deep network to detect breast cancer metastasis. For breast cancer detection, metastasis of lymph node in while slide images (WSIs) plays a critical role for its detection but is a great challenge due to large variation in size and appearance of WSIs. A spatially structured network (Spatio-Net) deep neural network by integrating with 2D Long-short term memory (2D-LSTM) was proposed by [41] to detect and tackle the metastasis problem in WSIs. Gao *et al.* [42] proposed a nonlinear state-space approach to track motion of common carotid artery (CCA) for early diagnosis of atherosclerotic disease. To estimate the motion trajectory of CCA wall from noisy ultrasound images, the unscented Kalman filter (UKF) was applied to solve the nonlinear state transfer function for evolving the state of target tissues. Moreover, to correct the biased displacement of the block during the motion tracking process, a time-variant control signal from mathematical models [43], [44] was applied.

In the past, researchers extracted various features from MRI images to detect and predict PCa. These features include texture, morphological, elliptic Fourier descriptors (EFDs), scale invariant feature transform (SIFT), local binary patterns (LBP), gray-level co-occurrence matrix (GLCM), Haar transform and statistical features etc. Texture features have been very promising for prostate detection in various studies including Perez *et al.* [45] work leading to the maximum AUC of 0.85 and Han *et al.* [46] work leading to sensitivity/specificity of above 90%. Recently, a combination of various features such as texture, morphological, SIFT, and EFDs coupled with robust machine learning methods has been used to detect PCa [47]. The highest reported accuracy in this study using individual features was 98.34% (AUC = 0.99), however the combination of texture, morphological, and EFDs led to accuracy of 99.71% (AUC = 1.00) using Gaussian kernel of support vector machines (SVM). For prognostic and diagnostic of Prostate specimen, different aspects are desired to be considered such as dimension, architectural pattern (poorly formed, cribriform, fused), sector (anterior/ posterior), tumor size, regional part (apex/mild/base), laterality (right/ left) and presence of extraprostatic extension. For proper detection of PCa, geometric features based on morphology are extracted for further analysis.

A probabilistic relationship between the variables [48], [49] can be illustrated using Bayesian networks via directed acyclic graphs (DAG). The DAG consists of nodes, denoting the clinical variables, and edges which connect the nodes

and represent the conditional dependencies among them. For establishing the network structure for better probabilistic relationship representation between the variables, different approaches and algorithms are used to search the possible networks. Recently, Machine learning has been widely used to analyze the highly complex and multi-dimensional data sets to compute the complicated tasks such as language processing, image processing [50], or radiological image analysis [51]. These techniques have been rapidly evolving and there is a great potential of the applications in clinical neuroscience. In this study, we used Bayesian networks to quantify the relationship between the morphological features used in prostate cancer detection [52]– [54].

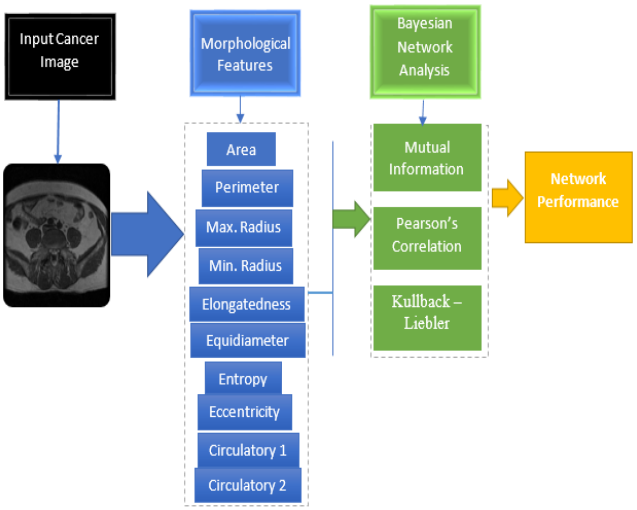


**FIGURE 1. Schematic Diagram of Bayesian Network analysis approach based on morphological features extracted from prostate cancer images.**

Fig. 1 shows schematic diagram of the proposed system. Image acquisition is the first step of the proposed system. In the second step, various morphological features are extracted from Prostate Cancer Imaging Database to quantify the shape/morphology of prostate tumors. In the third step, Bayesian Network analysis approach is used to develop a network of features (nodes) and to determine the strength of relationships between the features.

## II. MATERIAL AND METHODS

### A. DATA SET

The Dataset was taken from a publicly available database (http://prostatemrimagedatabase.com/index.html) provided by the National Center for Image Guided Therapy, Department of Radiology, Brigham and Women Hospital, Harvard Medical School, USA. The database was funded by National Institutes of Health and is available for research purposes. The database contains MRI of prostate cancer patients that are arranged with different series and examination description. We picked the images of Prostate and Brachytherapy with the last series for analysis. In particular, a total of 682 MRIs (prostate = 482, Brachytherapy = 200) were used for extracting features and employing machine learning classifiers to detect and predict PCa.

### B. FEATURES EXTRACTION

Feature extraction is an important step during classification and regression techniques. In the past, specific features have been extracted by the researchers for detecting any pathology in the cancer mammograms and other image databases. To detect colon cancer, [6], [55], [56] extracted the hybrid and geometric features. Hussain *et al.* [57] extracted acoustic and Mel frequency cepstral Coefficients (MFCC) features for emotion recognition in human speech, geometric and texture features [58], [59] for detection and recognition of human faces, complexity-based features [59], [60] for heart rate variability and to distinguish alcoholic and non-alcoholic subjects. Hussain *et al.* [47] recently extracted texture, morphological, SIFT and EFDs features and used different machine learning techniques and obtained outer performance result to detect the prostate cancer. By extracting morphological features, SVM Gaussian gives highest PCa detection performance with sensitivity (90.83%), specificity (87.10%), Positive Predictive Value (PPV) (90.84%), Negative Predictive Value (NPV) (86.86%), total accuracy (90.83%), and AUC (0.9896). Considering the effective performance of morphological features for various classification tasks, we have also selected morphological features to find the association among them by applying Bayesian Network approach. The main purpose of this study was to gain a deeper understanding of various morphological features and their associations using node and arc analysis.

### C. MORPHOLOGICAL FEATURES

Morphology represents the shape and structure of an image. It is a set of features which are computed to characterize the structural properties of tumor candidate regions. These features have been extensively used in the past for computer-aided diagnosis. For example, Khalvat *et al.* [61] extracted different morphological features for automated prostate cancer localization and detection. Biologist employed image analysis to quantify phenotypes, especially in high-throughput experiments [62]– [64]. Recent advancements in image analysis and automated microscopy enabled many treatment conditions to be tested in a single day, that help to systematically evaluate the morphologies of cells. Similarly, Kadir and Gleeson [65] extracted nodule size, morphology and smoking history as input variables to detect the lung cancer. Recent studies reveal that morphological features have been associated with the patient prognosis in lung cancer [66]– [68]. Isaza *et al.* [69] extracted different morphological features such as length, width, perimeter, thickness, area of transversal section, surface area, geometric mean diameter, sphericity, sphericity index, length index, Ferret diameter, compaction index, aspect ratio, and thinness ratio, and applied classification techniques for detection of seed of wild castor oil plants [70].

**TABLE 1.** Network performance analysis with DF of 4. RW = Relative Weight, OC = Over all Contribution, SNMI = Symmetric Normalized Mutual Information, SRMI = Symmetric Relative, DF = Degree of Freedom, PC = Pearson's Correlation.

| Parent | Child | KI/MI | RW | OC % | SNMI % | SRMI % | GKL TEST | PC |
|---|---|---|---|---|---|---|---|---|
| Area | Equidiameter | 1.0441 | 1 | 25.18 | 65.87 | 100.00 | 994.36 | 0.9978 |
| Max. Radius | Circulatory1 | 0.9154 | 0.877 | 22.08 | 57.76 | 92.13 | 871.84 | -0.8233 |
| Circulatory 1 | Entropy | 0.7161 | 0.686 | 17.27 | 45.18 | 73.71 | 682.02 | 0.7082 |
| Circulatory 1 | Elongatedness | 0.6804 | 0.652 | 16.41 | 42.93 | 72.38 | 648.04 | -0.7314 |
| Circulatory 2 | Area | 0.5275 | 0.505 | 12.72 | 33.28 | 48.08 | 502.34 | 0.7612 |
| Min Radius | Max. Radius | 0.0755 | 0.072 | 1.82 | 4.76 | 23.74 | 71.88 | 0.136 |
| Perimeter | Circulatory2 | 0.074 | 0.071 | 1.79 | 4.67 | 6.20 | 70.52 | -0.2862 |
| Entropy | Perimeter | 0.0642 | 0.062 | 1.55 | 4.05 | 5.90 | 61.12 | -0.2213 |
| Min Radius | Eccentricity | 0.0494 | 0.047 | 1.19 | 3.12 | 64.89 | 47.05 | 0.872 |

Likewise, morphological approach is employed in many image processing methodologies including [71]– [74] and [75]. The collection of non-linear operations (such as dilation, erosion, closing, opening, tophat filtering, and watershed transform etc.) are associated with the shape or features in an image are known as a morphological approach.

Researchers [76]– [82] proposed various feature extraction methods to grade Diabetic Macular Edema (DME) stages without segmenting exudates. Hunter *et al.* [82] proposed morphological features for automated grading of referral maculopathy and obtained classification performance with accuracy (97.01%), specificity (99.07%) and sensitivity (92.14) using 7 locality sensitive discriminant analysis (LSDA) features.

Xu *et al.* [83] extracted five morphological features including perimeter, area, eccentricity, equivalent diameter and ellipticity from each nucleus to capture the nuclear morphologies for detecting the melanocytic tumor on skin. Using all features a detection performance by employing SVM with linear kernel and regularization parameter C (1.0) was obtained with sensitivity (99.39%), specificity (96.98%), and precision (97.51%). Morphological features have been extracted from various image types to quantify the shape/morphology of images into a set of quantitative values for classification [52]– [54] and segmentation [84] purposes. The geometric and shape based features are mostly used to detect the masses present in the medical images [85].

The studies mentioned above lack in terms of the analysis of the magnitude and associations between different features. Our study provides an insight to the association among morphological features extracted from imaging database, thereby helping the researchers to adopt these features in detecting many chronic diseases. The morphologic features that we extracted include area, perimeter, max. radius, min. radius, Elongatedness, equi- diameter, entropy, eccentricity, circulatory 1, and circulatory 2 as described earlier [47], [86], [87]. The mathematical formulation and description of extracted morphological features from PCa are detailed in Table 2.

### D. BAYESIAN NETWORK ANALYSIS

Bayesian networks represent DAG, wherein nodes and arcs typically show cause and effect relationship between different variables [88]. The Bayesian networks topographic structure reflects the dependency of the variables and illustrates the probability distribution of certain tasks occurred in the specified conditions. Consider X= $\{X_1, X_2, X_3, \ldots\ldots, X_n\}$ a set of $n$ dimensional variables, then the Bayesian network is formally defined as a set of couplets $X = <G, P>$ where G denote the DAG in which each node denotes one the variable $X_1, X_2, X_3, \ldots, X_n$ and each arc represents the direct dependency relationship between these variables. Moreover, P denotes the set of parameters that quantify the network, contain the probabilities of each possible value xi for each variable Xi. By decomposing the joint probability P under hypothesis that each node is independent of its non-descendants can be computed using joint probability distribution function of the Bayesian Network as:

$$P(X) = P(X_1, X_2, X_3 \ldots\ldots., X_n) = \prod_{i=1}^{n} P(\frac{X_i}{X_{j(i)}}) \quad (1)$$

where $X_{j(i)}$ denote the set of parent variables of $X_i$for direct acyclic graph G. The Bayes theorem thus consequently enables to determine the posterior probability through inference of the variable of interest.

The variables of interest are extracted as morphological features from Prostate Cancer Database images. The Bayes Networks model analysis was performed using the BayesiaLab V7 software [89] by applying a set of supervised learning algorithms to search the optimal model. The information exchanged between target variables and any contaminant was computed using Shannon Entropy [90]. The Shannon Entropy of a discrete variable X is defined as follow:

$$H(X) = -\sum\nolimits_{x \epsilon X} p(X) log_2 p(X) \quad (2)$$

The difference between the conditional entropy of the given target (predicted variable) and marginal entropy of the target

**TABLE 2.** Morphological features and their mathematical formulae.

| Morphological Features | Mathematical Equations | Descriptions |
|---|---|---|
| Area (A) | Total number of pixels in a region-of-interest. | Total number of pixels in a region-of-interest. |
| Perimeter (P) | Total number of pixels at the boundary of region-of-interest. | Total number of pixels at the boundary of region-of-interest. |
| Maximum Radius (MAX_R) | The maximum distance between center and boundary of a region-of-interest. MAX(DISTANCE(C(x,y), BOUNDARY(x,y))) | To calculate maximum distance between the center of a region-of-interest to its boundary. C(x,y) is the center of the region-of-interest and BOUNDARY(x,y) is a pixel on the boundary of the region-of-interest. |
| Minimum Radius(MIN_R) | The minimum distance between center and boundary of a region-of-interest. MIN(DISTANCE(C(x,y), BOUNDARY(x,y))) | To calculate minimum distance between the center of a region-of-interest to its boundary. C(x,y) is the center of the region-of-interest and BOUNDARY(x,y) is a pixel on the boundary of the region-of-interest. |
| Eccentricity (ECT) | $\sqrt{1-\left(\frac{MIN\_R}{MAX\_R}\right)^2}$ | It is the ratio of major axis and minor axis. |
| Equivdiameter (EQD) | $\sqrt{4*\frac{Area}{\pi}}$ | It is used to calculate diameter of a circle which has same area as region-of-interest. |
| Elongatedness(EN) | $\left(\frac{Area}{(2*MAX\_R)^2}\right)$ | Elongatedness of a region-of-interest is ratio of its length to its thickness. |
| Entropy (ENTPY) | $\sum\left(p*log_2(p)\right)^2$ | It is a statistical measure of randomness which is used to characterize the texture of region-of-interest. |
| Circularity1 (C_1) | $\sqrt{\frac{Area}{\pi*MAX\_R^2}}$ | It is used to quantify the resemblance of a region-of-interest with circle. |
| Circularity1 (C_2) | $\sqrt{\frac{MIN\_R}{MAX\_R}}$ | It is used to quantify the resemblance of a region-of-interest with circle. |

variable is formally known as Mutual Information [90] and denote by I. Mathematically, the Mutual Information between the variable X and Y is defined by [91] as follow:

$$MI\,(X,Y) = H\,(X) - H(\frac{X}{Y}) \tag{3}$$

Which is equivalent to:

$$MI\,(X,Y) = \sum_{x\epsilon X}\sum_{y\epsilon X} p\,(X,Y)\,log_2\frac{p(X,Y)}{p\,(X)\,p(Y)} \tag{4}$$

Moreover, conditional Mutual Information (CMI) is defined as:

$$CMI\,(X,Y|Z) = \sum_{x\epsilon X}\sum_{y\epsilon X}\sum_{y|z\epsilon X} p\,(X,Y|Z) \times log_2\frac{p(X,Y|Z)}{p\,(X|Z)\,p(Y|Z)} \tag{5}$$

The joint probability distribution of X and Y is denoted by p (X, Y). The marginal distribution of X and Y is represented by p(X) and p(Y) respectively. For data representation in Gaussian distribution [92], [93], the n-dimensional Gaussian Distribution with |C| as determinant of covariance matrix of variables $X_1, X_2, X_3, \ldots, X_n$ [94] can be computed as:

$$H\,(X) = \log\,(2\pi e)^{\frac{n}{2}}\,|C|^{\frac{-1}{2}} \tag{6}$$

By mathematical transforming, the Mi and CMI2 can be computed as follow:

$$MI\,(X,Y) = \frac{1}{2}\log\frac{|C\,(X)\,| \times |C\,(X)\,|}{|C\,(X,Y)\,|} \tag{7}$$

CMI2 proposed to integrate interventional probability and Kullback—Leibler (KL) divergence [94] to correct the under-estimation of CMI [95], (8), shown at the bottom of the next page. CMI2 can be easily computed with the same hypothesis of the Gaussian distribution. A complete description and details of the computational process with mathematical formulation can be obtained in Zhang's work [93].

Pearson correlation coefficient (PCC) is a statistical method that measures the direction and strength of a linear relationship between two random variables [96]. PCC has most widely been used in many applications such as data analysis [97], classification [97], decision making and clustering [98], biological research [99], and finance analysis [100]. The PCC of two variables X and Y is formally defined as the covariance of the two variables divided by the product of their standard deviations [96]. Mathematically:

$$r_{XY} = \frac{\sum (X_i, \bar{X}) \sum (Y_i, \bar{Y})}{\sqrt{\sum (X_i, \bar{X})^2} \sqrt{\sum (Y_i, \bar{Y})^2}} \tag{9}$$

where $\bar{X} = \frac{1}{n} \sum_{i=1}^{N} X_i$ denote the mean of X, and $\bar{Y} = \frac{1}{n} \sum_{i=1}^{N} Y_i$ denote the mean of Y.

The coefficient $\mathbf{r_{XY}}$ ranges from -1 to 1 and is invariant to linear transformations of either variable. The PCC gives the strength of linear relationship between the two random variables X and Y. The positive sign denotes that two variables are directly correlated whereas negative sign denotes that they inversely related. When $\mathbf{r_{XY}} = 0$, then these variables are uncorrelated. When the value of $|\boldsymbol{r_{XY}}|$ is closer to 1, it indicates that there is a stronger relationship and closeness to a linear relation.

## III. RESULTS

In this study, we extracted ten morphological features, namely Equidiameter, area, Circulatory1, Circulatory2, perimeter, entropy, Elongatedness, max radius, min radius, and eccentricity from Prostate Cancer imaging database. The arc analysis was performed using MI, PC and KL as shown in Fig. 2. For node analysis, various factors were considered such as Bayes factor, node force, entropy, mean, normalized mean and reference state probability.

The greatest arc strength of 1.0441 was obtained using MI and KL between feature pairs (Equidiameter, Area) followed by 0.9154 (Circulatory1, Radius), 0.7161 (Circulatory1, Entropy), 0.6804 (Circulatory1, Elongatedness), 0.5275 (Area, Circulatory2), 0.0755 (Min. Radius, Max. Radius), 0.0740 (Circulatory2, Perimeter), 0.0642 (Entropy, Perimeter) and 0.0494 (Min. Radius, Eccentricity).

The Arc analysis using PC is depicted in Fig.3. The greatest Arc strength of 0.9987 was obtained between features pair (Equidiameter, Area) followed by 0.8720 (Min. Radius, Eccentricity), −0.8233 (Circulatory1, Radius), 0.7612 (Area, Circulatory2), −0.7314 (Circulatory1, Elongatedness), 0.7082 (Circulatory1, Entropy), −0.2862 (Circulatory2, Perimeter), −0.2213 (Entropy, Perimeter) and 0.1360 (Min. Radius, Max. Radius).

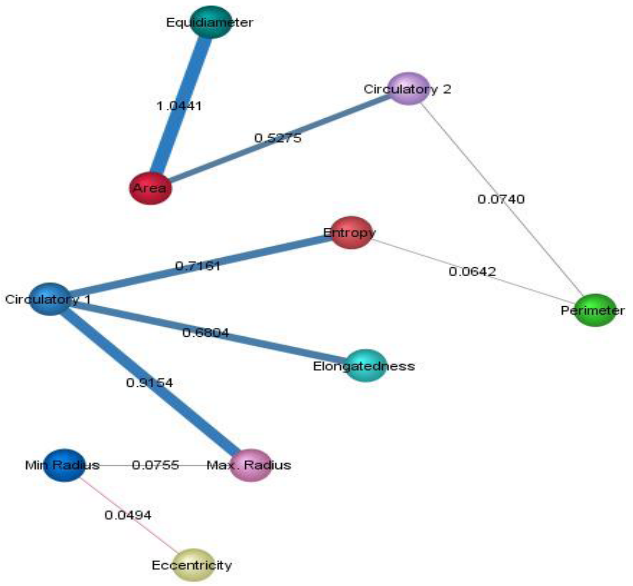


**FIGURE 2.** Arc Analysis using MI and KL methods.

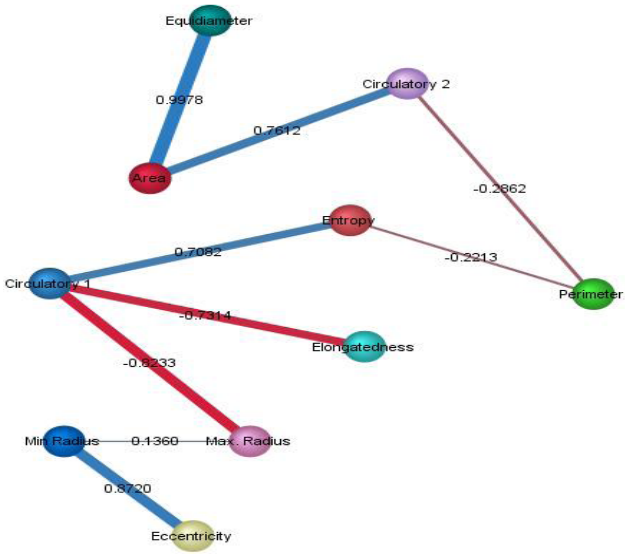


**FIGURE 3.** Arc Analysis using PC.

The network analysis with a node (size) using Bayes factor and Arc using PC of Morphological features extracted from Prostate Cancer Images Database is reflected in Fig. 4. The strengths of Arcs between the adjacent nodes (morphological features) is reflected similarly as shown in Fig. 3 for PC.

The greatest node force was obtained for Circulatory1 followed by Area, Equidiameter, Max. Radius, Entropy, Elongatedness, Circulatory 2, and Perimeter as shown in Fig. 5. The arc strengths are obtained similarly as of PC between each adjacent node.

$$CMI2\,(X, Y|Z) = \sum_{X,Y,Z} p(X, Y, Z) ln \frac{p(X, Y, Z)}{p(X, Z) \sum_{x} p\,(Y|X, Z)\, p\,(X) + p(Y, Z) \sum_{y} p\,(X|Z, Y)\, p(Y)} \tag{8}$$

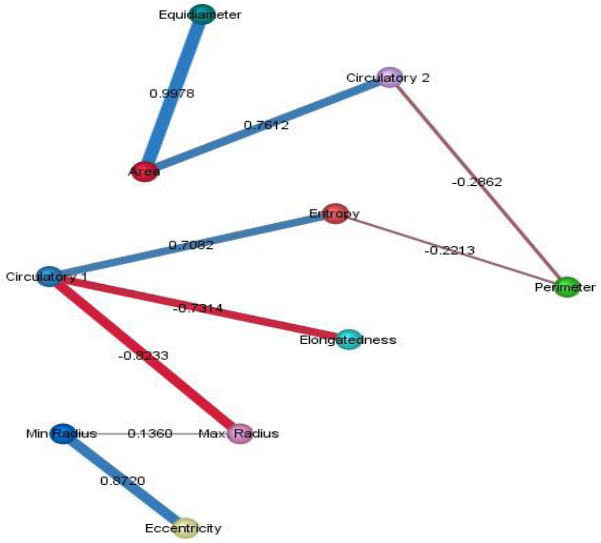


**FIGURE 4.** Node Analysis using Bayes Factor – Arc Analysis using PC.

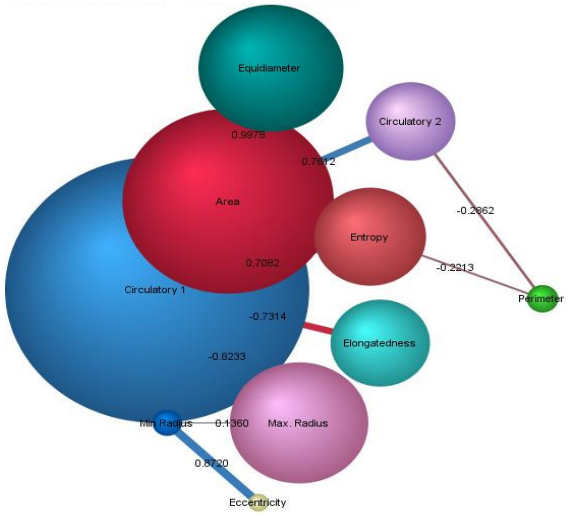


**FIGURE 5.** Network Node Analysis (Node Force) – Arc Analysis using PC.

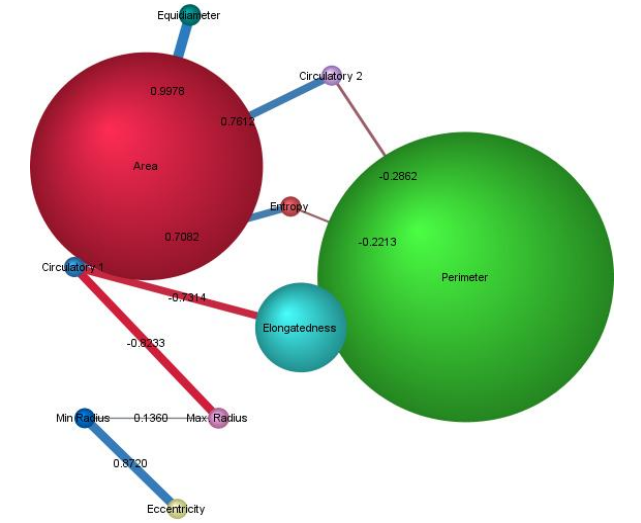


**FIGURE 6.** Network Node analysis using Mean and Arc analysis using PC.

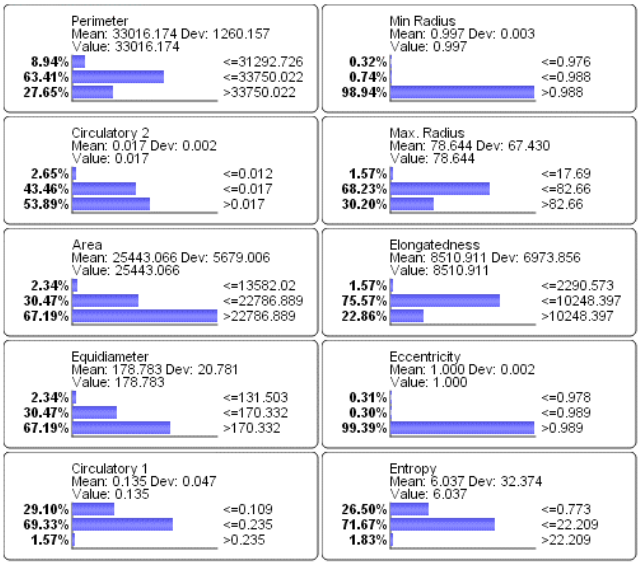


**FIGURE 7.** Impact of interaction on the proportion of morphological features.

The greatest node size was obtained for Perimeter followed by Area, Elongatedness, Equidiameter, Circulatory1, Circulatory 2, Min. radius, Max. radius, Eccentricity and Entropy as shown in Figure 6.

Based on the different measures, the Bayesian Network showed performance as reflected in Table 1. The arc strength between different nodes (*Paren* → *Child*) of KL, MI and PC is reflected in Table 1 and Figures above. The highest performance was obtained between nodes (*Area* → *Equidiameter*) as KL divergence (1.0441), RW (1), OC (25.18%), MI (1.0441), SNMI (65.87%), SRMI (100%), GKL test (994.3664), P-value (0.00%), PC (0.9987) followed by (*Max.Radius* → *Circulatory*1) as KL (0.9154), RW (0.877), OC (22.08%), MI (0.9154), SNMI (57.76%), SRMI (92.13%), GKL (871.8372), P-value (0.00%), PC (-0.823); (*Circulatory*1 → *Entropy*) as KL (0.7161), RW (0.686), OC (17.27%), MI (0.7161), SNMI (45.18%), SRMI (73.71%), GKL (682.0175), P-value (0.00%), PC (0.7082)

The next best performance was observed for (*Circulatory*1 → *Elongatedness*) followed by (Max. Radius → Circulatory 1), (Circulatory 1 → Entropy), (Circulatory 1 → Elongatedness), (Circulatory 2 → Area), (Min. Radius → Max. Radius), (Perimeter → Circulatory 2), (Entropy → Perimeter), (Min. Radius →Eccentricity) for which the arc strength for MI, KI, PC, over all contribution (OC), Symmetric Normalized Mutual Information (SNMI), Symmetric Relative (SRMI) values are reflected accordingly for each pair of features in Table1.

The variable Perimeter has a mean of 33016.174 and deviation of 1260.157 with probability of 63.41% in the state <= 33750.022. The variable Minimum Radius has

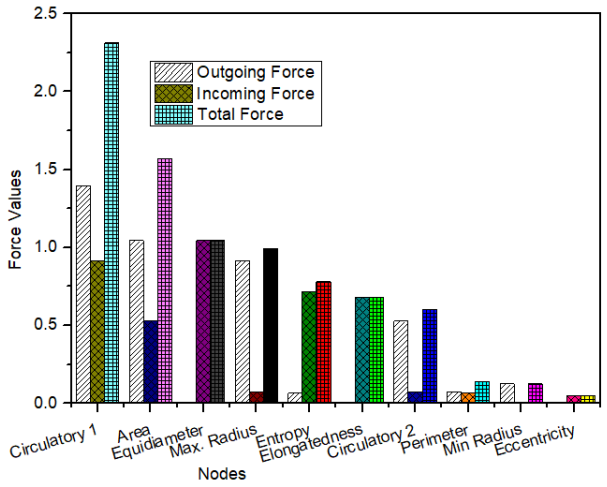


**FIGURE 8.** Node force Analysis for each extracted morphological feature.

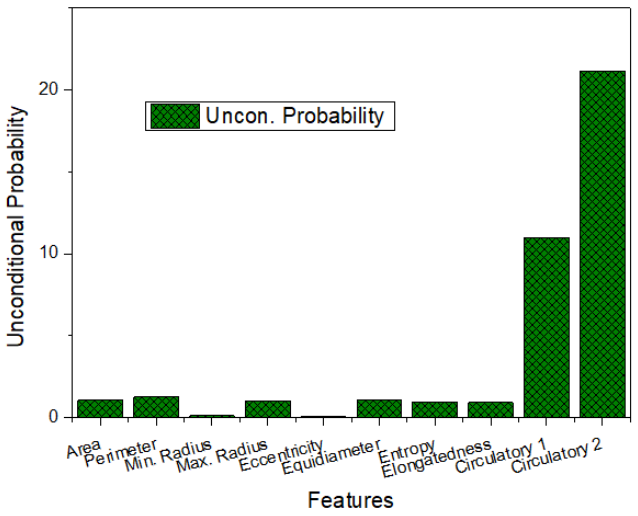


**FIGURE 9.** Individual Unconditional Probability of Nodes.

mean of 0.997 and deviation of 0.003 with probability of 98.94% in the state >0.988. The variable Circulatory 2 has probability of 53.89% of being in the state > 0.017, 43.46% in the state of <= 0.017 and only 2.65% in the state of <= 0.012. Maximum radius has mean of 78.644, standard deviation of 67.430 has the probability of 68.23% being in the state <= 82.66. Area has mean value of 25443.066 and deviation of 5679.006 has 67.19% probability in the state of > 22786.889. The variable Elongatedness has mean of 8510.911 and deviation of 6973.573 has the probability of 75.57% in the state <= 10248.397. The variable Equidiameter has mean of 178.783 and deviation of 20.781 with probability of 67.19% in the state of > 170.332. The Eccentricity variable has mean of 1 and deviation of .002 with probability of 99.39% in the state of 0.989. Variable Circulatory 1 has mean of 0.135 and deviation of 0.047 with probability of 69.33% in the state of 0.235. The Entropy variable has mean 6.037 and deviation of 32.374 with probability 71.67% in the state 22.209.

The Node force for each morphological feature is computed (Fig. 8). The greatest outgoing force was obtained at node Circulatory1 (1.3966) followed by Area (1.0441), Maximum Radius (0.9154), Circulatory2 (0.5275), Minimum Radius (0.1249), Perimeter (0.0740) and Entropy (0.0642). The nodes Equidiameter, Elongatedness, and Eccentricity showed zero outgoing force. Similarly, the greatest incoming node force was obtained at node Equidiameter (1.0441) followed by Circulatory1 (0.9154), Entropy (0.7161), Elongatedness (0.6804), Area (0.5275), Max. Area (0.0755), Circulatory2 (0.0740), Perimeter (0.0642), Eccentricity (0.0494). The Min. Radius showed zero incoming force. The greatest net force was obtained at node Circulatory1 (2.3120) followed by Area (1.5715), Equidiameter (1.0441), Maximum Radius (0.9909), Entropy (0.7803), Elongatedness (0.6804), Circulatory2 (0.6015), Perimeter (0.1382), Minimum Radius (0.1249) and Eccentricity (0.0494).

Fig. 9 depicts the unconditional probability computed for each individual node. The greatest value was obtained at node Circulatory2 (21.1529) followed by Circulatory1 (10.9866), Perimeter (1.2362), Area & Equidiameter (10.0441), Maximum radius (1.0007), Entropy (0.9567), Elongatedness (0.8958), Minimum Radius (0.1010) and Eccentricity (0.0574).

An inference was applied based on Bayesian approach by representing joint probability distribution as Bayesian network. The Bayesian network nodes represent variables of interest (e.g. Area, perimeter, Equidiameter, entropy, circulatory, radius, eccentricity, Elongatedness etc.) and causal and statistical dependencies among the variables are represented by the links. These dependencies in the network are quantiled by the conditional probabilities for each give node as given by its parent. A posterior probability can be supported by the network of any subset of variables given evidence about any other subset. The inference can be performed by introducing the evidences that the sets variable in known states, and subsequently computed probabilities of interest are conditioned on this evidence. By combining the probability rule with the Bayes rule make for a complete reasoning system, one which includes traditional deductive logic as a special case [101].

The Bayesian networks were initially proposed in late 1970s with the motivation to model bottom-up (perceptual) and top-down (semantic) combination of evidence reading. This bidirectional inference capability combined with the rigorous probabilistic foundation made the Bayesian network a rapid emergence and choice for uncertain reasoning in expert systems and artificial intelligence by replacing earlier ad-hoc rule-based systems.

BayesiaLab is facilitates us to visualize the quantitative part of the network beyond the visual inspection of the network structure. Bayes networks provide a detailed analysis of domain knowledge for variables of interest through compact representation of joint probability distribution. These networks are inherently probabilistic, evidences and inferences are represented as distributions inference can be performed with partial evidence. Moreover, Bayes networks can

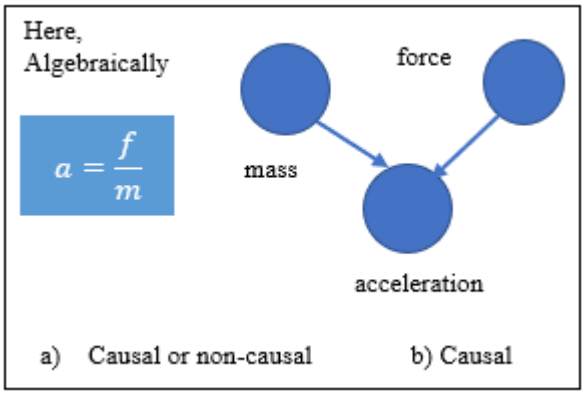


**FIGURE 10.** Algebraic and Bayesian network relationship a) Algebraic relation represent causal or non-causal, b) Bayes network approach represent causal relations only.

formally encode a causal direction, which algebra cannot do. e.g. According to Newton's second law of motion, a = f/m, where a=acceleration, f = force and m = mass of an object as reflected in Figure 10.

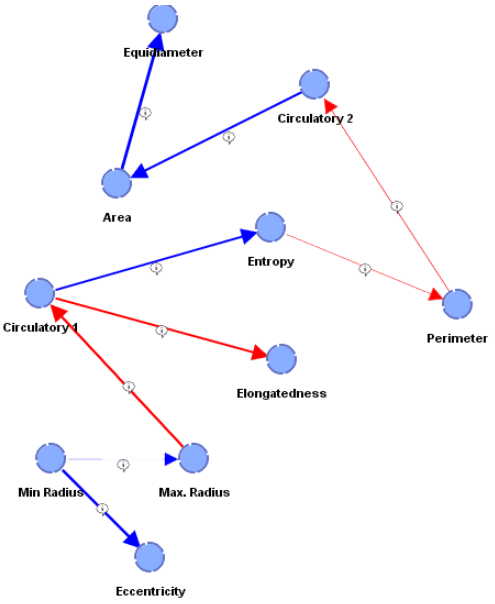


**FIGURE 11.** Association among Morphological features using Pearson's' Correlation.

In Figure 11, the associations among the morphological features are quantified in terms of PC. The thickness of each is proportional to the PC between the connected nodes. The red and blue colors indicate negative and positive correlations, respectively.

The dependencies among the nodes are reflected using the arrow symbols i.e. (Parent→ child nodes) such as

$$(area \rightarrow equidiameter),$$
$$(circulatory2 \rightarrow area),$$
$$(perimeter \rightarrow circulatory2),$$
$$(entropy \rightarrow perimeter),$$
$$(ciculatory1 \rightarrow elongatedness),$$
$$(circulatory1 \rightarrow entropy),$$
$$(Max.Radius \rightarrow circulatory1),$$
$$(Min.Radius \rightarrow Max.Radius)$$
$$and\ (Min.Radius \rightarrow eccentricity).$$

There is a strong positive correlation between nodes such as (area, Equidiameter), (circulatory2, area), (circulatory1, entropy), and (Min. radius, eccentricity) reflected by blue lines in Figure 11. Moreover, a strong negative correlation was found between nodes such as (circulatory1, Elongatedness), and (Max. radius, circulatory1). Likewise, smaller negative correlation was found between the nodes (perimeter, circulatory2), and (entropy, perimeter). A partial smaller positive correlation was found between the nodes (Min. radius, max. radius).

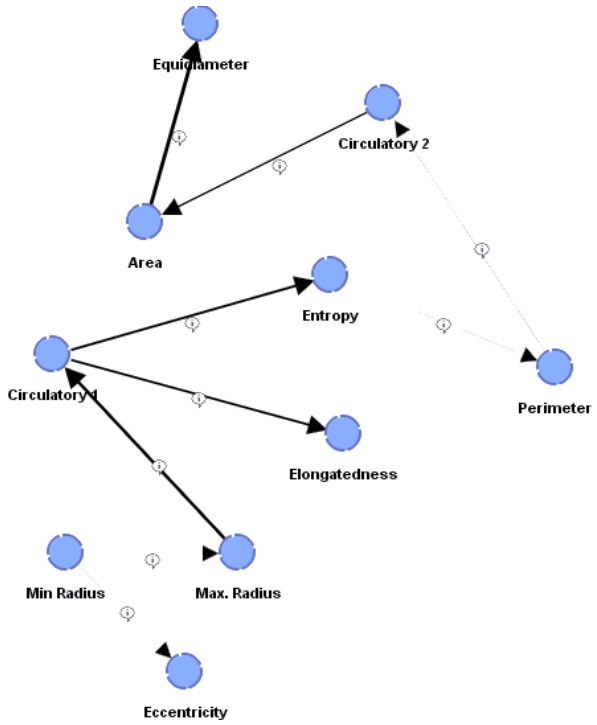


**FIGURE 12.** Association among Morphological features using MI and KL methods.

Figure 12 reflect the association among nodes using MI and KL methods. A stronger strength of relation was found between the nodes. i.e. (area → equidiameter), (circulatory1, max. radius). A moderate strength was obtained between the nodes (circulatory2 → area), circulatory1 → entropy), (circulatory1 → elongatedness). Similarly, a very minor strength was found between the nodes (perimeter, circulatory2), (max. radius, min. radius), (min. radius → eccentricity).

Figure 13 depicts the automatically produced three different clusters using BayesiaLab based on morphological features extracted from prostate cancer images represented by green, yellow and pink nodes to denote the association and relevancy among the nodes. The green nodes cluster

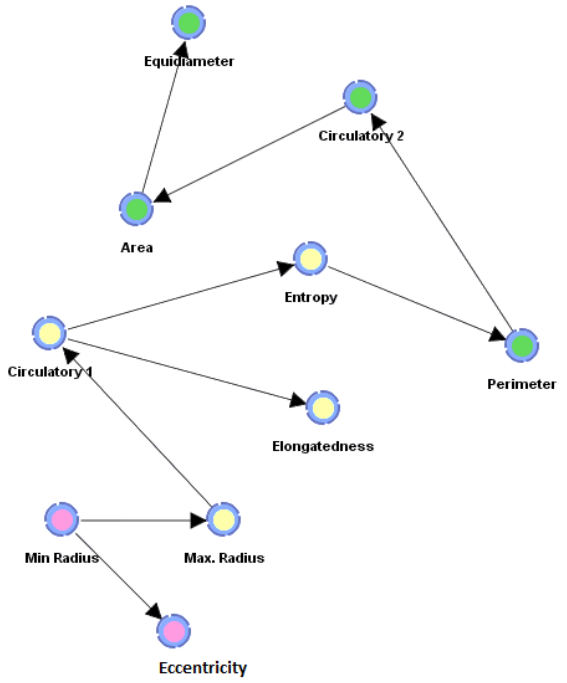


**FIGURE 13.** Bayesian Network clustering association between Morphological features of Prostate Cancer images.

comprised of (area, Equidiameter, circulatory2, perimeter) followed by the yellow nodes cluster (circulatory1, entropy, Elongatedness, max. radius) and pink nodes cluster (min. radius, Eccentricity).

The MI and KL demonstrate similar association between the nodes. The greatest association using MI and KL is obtained between nodes (Area, Equidiameter) followed by (Circulatory 1, Max. Radius), (Circulatory 1, Entropy), (Circulatory 1, Elongatedness) etc. By using Pearson's correlation method, the strongest association is obtained between nodes (Area, Equidiameter) followed by (Min. Radius, Eccentricity), (Area, Circulatory 2), (Circulatory 1, Min. Radius), (Circulatory 1, Entropy), and (Circulatory 1, Elongatedness) etc. The negative sign indicates the inverse relationship and the value indicates the degree of association between the variables. Moreover, the network analysis based on the node size and the arc strength was evaluated. The analysis using Node size (Bayes factor) and arc analysis using PC is performed which give similar node size using Bayes factor where arc association is obtained similarly as of using PC. Using node force as node size, the greatest size is obtained of node Circulatory 1, followed by Area, Max. Radius, Elongatedness, Entropy, Equidiameter etc. Whereas, based on node mean value, the greatest values of the node are obtained at Perimeter followed by Area, Elongatedness etc. Similarly, the greatest contribution between nodes was obtained as (Area, Equidiameter), followed by (Max. Radius, Circulatory 1), (Circulatory 1, Entropy), (Circulatory 1, Elongatedness), (Circulatory 2, Area) etc. Moreover, all possible parent – child pairs give a very highly significant p-value $<0.00\%$. The impact of each individual node is computed. The interaction distribution for each individual node at various state was computed as reflected in Figure 7. The incoming, outgoing and net force was computed. The greatest outgoing force is obtained at node Circulatory 1 followed by Area and Max. Radius etc. The greatest incoming force is obtained at Equidiameter, followed by Circulatory 1, Entropy and Elongatedness etc. The greatest individual unconditional entropy is obtained at node Circulatory 2 followed by Circulatory 1, Perimeter, Area, Equidiameter, Max. Radius, and Entropy.

## IV. DISCUSSION AND CONCLUSION

Nodes of the DAG system i.e. morphological features represent clinical predictors, whereas edges between different nodes represent probabilistic relationships. This approach has advantages than the traditional approaches because it gives an insight into the probabilistic relationship by showing the influence of variables among each other. In this research, the relationship is developed among features extracted from Prostate Cancer as discussed in [47]. The Bayesian network approaches have another distinctive characteristic that it is inspired by the biological structure of nervous tissues, in which neurons process synaptic input and subsequently communicate with each other. Bayesian network approaches have been widely used in different application such as image processing, handwriting or even voice recognition. Bayesian network approaches have widely been used in a variety of applications such as prior biochemical knowledge modeling [102], scientific disciplines using machine learning [48], [103], [104], epidemiology [13], [103] etc. These approaches are like the statistical methods being widely used to study the Cancer. However, this approach has the advantage to model the variables simultaneously for understanding association among multiple variables and selecting variable for further univariate analysis.

The strength of relationship between any pair of variables can be estimated using correlation analysis. The covariance measure depends on the variability of each of two variables. To determine the strength between two variables, different correlation coefficient methods have been applied such as Kendall [105], Spearman [106], and Reimann *et al.* [107]. All these methods output numbers in the range $[-1, +1]$ to express that how closely the two variables are related. A perfect correlation (positive or negative) is represented by $\pm 1$ and 0 indicates that there is no systematic relationship between the two variables. A correlation of $\pm 0.5$ is usually considered as significant relationship.

To compare the Bayesian network structure, Bayesialab uses the minimum description length of candidate in its score-based algorithm [91]. The complexity of the network is modified by structural coefficient (SC) through weighting the structure encoding (in bits) of the Bayesian network.

A comprehensive network analysis is performed to find the relationship among the descriptors in the selected network and to study the influence of individual descriptors on

Prostate cancer prediction. To examine the in-depth relationship between the variables, the highest and lowest values of PC, MI, KL divergence, and node force between variables are observed globally on the network. The probabilistic dependence between the nodes in the network is computed using Mutual information. Moreover, PC is used to compute the linear strength of relationship between the variables. The joint relationship between two variables in the network compared to an assumption of independence is determined using KL divergence to measure the information gain. The KL divergence input is summed by node force to a node and output by the node. The highest node force shows that there is more direct relationship and greater dependence of node with each other.

Bayesian inference networks are used in variety of applications to determine the association among the nodes involved in the network. First, these networks have been proven to be useful to describe the processes composed of locally interacting components when the value of each component directly depends on the values of a relatively small number of components. Second, statistical foundations from observations for learning Bayesian networks, and computational algorithms have successfully been used in many applications. Finally, Bayesian networks have been used for providing causal relationships. Mathematically, these networks have strictly been used in terms of probabilities and conditional independence statements, a direct connection can then be made between the notion of direct causal influence and this characterization [108]– [110].

Correlation is one of the most common indices which is used in pattern recognition, data analysis, decision making and machine learning etc. to measure the collinearity of two variables. Karl Pearson proposed different correlation coefficient which have been extended into different fuzzy circumstances. In literature, researchers explored different types of correlation coefficients such as fuzzy correlation, Pearson's correlation and correlation coefficients [111], [111]– [115], hesitant fuzzy correlation and correlation coefficients [116], [117] and the intuitionistic fuzzy correlation and correlation coefficients [118]– [123]. In this study, we used Pearson's correlation coefficient.

Pearson's Correlation (PC) [124] is the most common method used to measure the relationship between different variables, however, it can meaure only linear relationship. To measure the independence between two random variables, mutual information (MI) is commonly used to measure nonlinear relationship and is more appropirate to identify those relationship between datasets which might go undetected using simple correlation [125]. The applications of MI include the use of independent component analysis [126] and analysis of both small and high dimensional data sets [127]– [129]. MI is drived from Shannon's entropy theory and has similar characterstics in resemblence with Shannon entropy and is applied successfully in the field of information theory [130], [131]. Pluim *et al.* [132] proposed an algorithm for computation of MI with high dimensional variables and successfully been applied in medical imaging registering .

The main objective of this study is to conduct a deeper analysis to find the relationship, and a degree of association between variables extracted from the images. We extracted morphological features from the Prostate Cancer imaging database, and then employed Bayesian Network analysis using BayesiaLab to find and quantify the associations between nodes for further arc and node analysis. This analysis informs us about the strength of each feature by itself and also the strength of association between different features. The Bayesian network approach methods including MI, PC, and KL were used to find the relationship between the nodes using BayesiaLab Software. For a broader understanding of the relationship between the nodes in the network of morphological features, we computed node force, node size, arc strength and impact of interaction among the nodes by employing MI, PC and KL divergence, and node force between variables was examined globally on the network. The probabilistic dependencies between the nodes in the network were determined using mutual information. A linear strength of relationship between the variables of interest was determined using PC. Moreover, information gain between two variables by assuming a joint relationship in the network compared to an assumption of independence was measured using KL divergence. Node force sums the KL divergence input to a node and output by the node. The highest node force denotes that there is a more direct relationship and greater dependence with other nodes.

Bayesian networks perform the relationship analysis among the variables of interest, whereas for deterministic models, it is difficult to establish and interpret the rules and due to complexity devastate understanding of the processes and models being represented. Moreover, Bayesian network approach can decompose the complex multivariate problems into graphical networks by visualizing and supporting bidirectional inferences under various levels of uncertainty. Likewise, the Bayesian networks have probabilistic focus which is conducive to improvements in quantification and structuring because the knowledge and evidences improve over time. The interaction between the variables using the coupling with subjective interpretation of probability preserves the focus on missing information and inaccuracy from deficient knowledge of true relationships.

We employ different Bayesian network inference approaches by computing the joint probability distributions. The arcs between the nodes characterize the probabilistic dependencies between the morphological features and their association is represented by the strength of relationship denoted by bold solid lines, dashed lines and smaller lines with different color representations. The strength is also reflected in terms of probabilistic values shown on the arcs. Moreover, causal relationships are represented by head and tails to represent the causal information, where arcs represent the direct causal influences such as a variable manipulated

at the tail of an arc will cause a change in the variable at the head of the arc mostly in all circumstances. The stronger strength of relations and node forces in our study is indicative of the fact that these features are rich enough to predict Prostate cancer. Recently, Hussain *et al.* [47] 2018 extracted different features to detect the Prostate cancer, however the study was lacking in terms of detailed analysis of the associations between different features. The associations discovered in this study will provide deeper insight into the biology of prostate cancer and will aid in detecting the cancer at an earlier stage. In the recent study, the association was computed using Bayesian network approaches among the morphological features. In future, we intend to quantify these associations in other feature categories as well such as texture, SIFT, EFDs and entropy-based features extracted from Prostate cancer and other cancer types. We also like to explore the associations between age, gender and other demographic information.

Using Bayesian network inference approach, we found important associations among the morphological features extracted from prostate cancer images which can be used for hypothesis generation. These studies required to investigate the significance of these novel associations, and the validity of these associations is supported by the presence of many well-known documented and self-evidence connections within overall Bayesian inference Network approaches. The research reported in this paper was to reflect the relationship between and among the various variables (features) extracted from Prostate Cancer. This will give an insight for deeper analysis of association and strength of the relationship between the features that may lead towards higher detection rate for Prostate Cancer and effectively improve the evaluation performance.

## ACKNOWLEDGMENT

*(Lal Hussain, Amjad Ali, and Saima Rathore contributed equally to this work.)*

## REFERENCES

[1] M. Arnold *et al.*, "Recent trends in incidence of five common cancers in 26 European countries since 1988: Analysis of the European cancer observatory," *Eur. J. Cancer*, vol. 51, no. 9, pp. 1164–1187, 2015.

[2] R. L. Siegel, K. D. Miller, and A. Jemal, "Cancer statistics, 2018," *CA, Cancer J. Clin.*, vol. 68, no. 1, pp. 7–30, Jan. 2018.

[3] M. F. Leitzmann and S. Rohrmann, "Risk factors for the onset of prostatic cancer: Age, location, and behavioral correlates," *Clin. Epidemiol.*, vol. 4, no. 1, pp. 1–11, 2012.

[4] F. Albright *et al.*, "Prostate cancer risk prediction based on complete prostate cancer family history," *Prostate*, vol. 75, no. 4, pp. 390–398, 2015.

[5] K. Hemminki, "Familial risk and familial survival in prostate cancer," *World J. Urol.*, vol. 30, no. 2, pp. 143–148, 2012.

[6] S. Rathore, M. Hussain, and A. Khan, "Automated colon cancer detection using hybrid of novel geometric features and some traditional features," *Comput. Biol. Med.*, vol. 65, pp. 279–296, Mar. 2015.

[7] K. K. Yu and H. Hricak, "Imaging prostate cancer," *J. Urol.*, vol. 38, no. 1, pp. 59–85, 2000.

[8] B. E. Sirovich, L. M. Schwartz, and S. Woloshin, "Screening men for prostate and colorectal cancer in the United States," *J. Amer. Med. Assoc.*, vol. 289, no. 11, p. 1414, 2003.

[9] M. Sieverding, U. Matterne, L. Ciccarello, and H.-J. Luboldt, "Prostatakarzinomfrüherkennung in Deutschland," *Urologe*, vol. 47, no. 9, pp. 1233–1238, 2008.

[10] E. C. Serefoglu, S. Altinova, N. S. Ugras, E. Akincioglu, E. Asil, and M. D. Balbay, "How reliable is 12-core prostate biopsy procedure in the detection of prostate cancer?" *Can. Urol. Assoc. J.*, vol. 7, nos. 5–6, pp. E293–E298, 2013.

[11] R. Kvåle *et al.*, "Concordance between Gleason scores of needle biopsies and radical prostatectomy specimens: A population-based study," *BJU Int.*, vol. 103, no. 12, pp. 1647–1654, 2009.

[12] T. Hambrock *et al.*, "Prospective assessment of prostate cancer aggressiveness using 3-T diffusion-weighted magnetic resonance imaging–guided biopsies versus a systematic 10-core transrectal ultrasound prostate biopsy cohort," *Eur. Urol.*, vol. 61, no. 1, pp. 177–184, 2012.

[13] M. A. Bjurlin *et al.*, "Optimization of prostate biopsy: The role of magnetic resonance imaging targeted biopsy in detection, localization and risk assessment," *J. Urol.*, vol. 192, no. 3, pp. 648–658, 2014.

[14] C. K. Kim, "Magnetic resonance imaging-guided prostate biopsy: Present and future," *Korean J. Radiol.*, vol. 16, no. 1, pp. 90–98, 2015.

[15] C. K. Kim and B. K. Park, "Update of prostate magnetic resonance imaging at 3 T," *J. Comput. Assist. Tomogr.*, vol. 32, no. 2, pp. 163–172, 2008.

[16] C. M. A. Hoeks *et al.*, "Prostate cancer: Multiparametric MR imaging for detection, localization, and staging," *Radiology*, vol. 261, no. 1, pp. 46–66, 2011.

[17] P. Puech *et al.*, "Prostate cancer diagnosis: Multiparametric MR-targeted biopsy with cognitive and transrectal US–MR fusion guidance versus systematic biopsy—Prospective multicenter study," *Radiology*, vol. 268, no. 2, pp. 461–469, 2013.

[18] B. K. Park *et al.*, "Prospective evaluation of 3-T MRI performed before initial transrectal ultrasound–guided prostate biopsy in patients with high prostate-specific antigen and no previous biopsy," *Amer. J. Roentgenol.*, vol. 197, no. 5, pp. 876–881, 2011.

[19] X. Zhen, Y. Yin, M. Bhaduri, I. Ben Nachum, D. Laidley, and S. Li, "Multi-task shape regression for medical image segmentation," in *Proc. Int. Conf. Med. Image Comput.-Assist. Intervent*, 2016, pp. 210–218.

[20] X. He, A. Lum, M. Sharma, G. Brahm, A. Mercado, and S. Li, "Automated segmentation and area estimation of neural foramina with boundary regression model," *Pattern Recognit.*, vol. 63, pp. 625–641, Mar. 2017.

[21] J. Chen, H. Zhang, W. Zhang, X. Du, Y. Zhang, and S. Li, "Correlated regression feature learning for automated right ventricle segmentation," *IEEE J. Transl. Eng. Heal. Med.*, vol. 6, 2018, Art. no. 1800610

[22] X. Qin, Z. Cong, L. V. Halig, and B. Fei, "Automatic segmentation of right ventricle on ultrasound images using sparse matrix transform and level set," *Proc. SPIE*, vol. 8669, p. 86690Q, Mar. 2013.

[23] M. R. Avendi, A. Kheradvar, and H. Jafarkhani, "Automatic segmentation of the right ventricle from cardiac MRI using a learning-based approach," *Magn. Reson. Med.*, vol. 78, no. 6, pp. 2439–2448, Dec. 2017.

[24] D. Grosgeorge, C. Petitjean, J.-N. Dacher, and S. Ruan, "Graph cut segmentation with a statistical shape model in cardiac MRI," *Comput. Vis. Image Understand.*, vol. 117, no. 9, pp. 1027–1035, 2013.

[25] W. Bai, W. Shi, H. Wang, N. S. Peters, and D. Rueckert, "Multiatlas based segmentation with local label fusion for right ventricle MR images," *Image*, vol. 6, p. 9, Jan. 2012.

[26] H. Zhang, A. Wahle, R. K. Johnson, T. D. Scholz, and M. Sonka, "4-D cardiac MR image analysis: Left and right ventricular morphology and function," *IEEE Trans. Med. Imag.*, vol. 29, no. 2, pp. 350–364, Feb. 2010.

[27] J. Ringenberg, M. Deo, V. Devabhaktuni, O. Berenfeld, P. Boyers, and J. Gold, "Fast, accurate, and fully automatic segmentation of the right ventricle in short-axis cardiac MRI," *Comput. Med. Imag. Graph.*, vol. 38, no. 3, pp. 190–201, Apr. 2014.

[28] C. Petitjean *et al.*, "Right ventricle segmentation from cardiac MRI: A collation study," *Med. Image Anal.*, vol. 19, no. 1, pp. 187–202, 2015.

[29] B. Kong, Y. Zhan, M. Shin, T. Denny, and S. Zhang, "Recognizing end-diastole and end-systole frames via deep temporal regression network," in *Proc. Int. Conf. Med. Image Comput.-Assist. Intervent*, 2016, pp. 264–272.

[30] W. Zhang *et al.*, "Deep convolutional neural networks for multi-modality isointense infant brain image segmentation," *NeuroImage*, vol. 108, pp. 214–224, Mar. 2015.

[31] H.-C. Shin, L. Lu, L. Kim, A. Seff, J. Yao, and R. M. Summers, "Interleaved text/image deep mining on a large-scale radiology database," in *Proc. IEEE Conf. Comput. Vis. Pattern Recognit.*, Jun. 2015, pp. 1090–1099.

[32] H. Greenspan, B. V. Ginneken, and R. M. Summers, "Guest editorial deep learning in medical imaging: Overview and future promise of an exciting new technique," *IEEE Trans. Med. Imag.*, vol. 35, no. 5, pp. 1153–1159, Mar. 2016.

[33] A. S. Rodin and E. Boerwinkle, "Mining genetic epidemiology data with Bayesian networks I: Bayesian networks and example application (plasma apoE levels)," *Bioinformatics*, vol. 21, no. 15, pp. 3273–3278, Aug. 2005.

[34] J. Yu, V. A. Smith, P. P. Wang, A. J. Hartemink, and E. D. Jarvis, "Advances to Bayesian network inference for generating causal networks from observational biological data," *Bioinformatics*, vol. 20, no. 18, pp. 3594–3603, Dec. 2004.

[35] N. Friedman, M. Linial, I. Nachman, and D. Pe'er, "Using Bayesian networks to analyze expression data," *J. Comput. Biol.*, vol. 7, nos. 3–4, pp. 601–620, 2000.

[36] R. Jansen, "A Bayesian networks approach for predicting protein-protein interactions from genomic data," *Science*, vol. 302, no. 5644, pp. 449–453, Oct. 2003.

[37] J. R. Bradford, C. J. Needham, A. J. Bulpitt, and D. R. Westhead, "Insights into protein–protein interfaces using a Bayesian network prediction method," *J. Mol. Biol.*, vol. 362, no. 2, pp. 365–386, Sep. 2006.

[38] K. Sachs, O. Perez, D. Pe'er, D. A. Lauffenburger, and G. P. Nolan, "Causal protein-signaling networks derived from multiparameter single-cell data," *Science*, vol. 308, no. 5721, pp. 523–529, Apr. 2005.

[39] N. Friedman, "Inferring cellular networks using probabilistic graphical models," *Science*, vol. 303, no. 5659, pp. 799–805, Feb. 2004.

[40] M. Rouprêt *et al.*, "A comparison of the performance of microsatellite and methylation urine analysis for predicting the recurrence of urothelial cell carcinoma, and definition of a set of markers by Bayesian network analysis," *BJU Int.*, vol. 101, no. 11, pp. 1448–1453, Jun. 2008.

[41] B. Kong, X. Wang, Z. Li, Q. Song, and S. Zhang, "Cancer metastasis detection via spatially structured deep network," in *Proc. Int. Conf. Inf. Process. Med. Imag.*, 2017, pp. 236–248.

[42] Z. Gao *et al.*, "Motion tracking of the carotid artery wall from ultrasound image sequences: A nonlinear state-space approach," *IEEE Trans. Med. Imag.*, vol. 37, no. 1, pp. 273–283, Jan. 2018.

[43] J. Stoitsis, S. Golemati, E. Bastouni, and K. S. Nikita, "A mathematical model of the mechanical deformation of the carotid artery wall and its application to clinical data," in *Proc. 29th Annu. Int. Conf. IEEE Eng. Med. Biol. Soc.*, Aug. 2007, pp. 2163–2166.

[44] S. Golemati, J. S. Stoitsis, A. Gastounioti, A. C. Dimopoulos, V. Koropouli, and K. S. Nikita, "Comparison of block matching and differential methods for motion analysis of the carotid artery wall from ultrasound images," *IEEE Trans. Inf. Technol. Biomed.*, vol. 16, no. 5, pp. 852–858, Sep. 2012.

[45] I. M. Perez *et al.*, "Diffusion weighted imaging of prostate cancer: Prediction of cancer using texture features from parametric maps of the monoexponential and kurtosis functions," in *Proc. IPTA*, vol. 1, 2016, pp. 1–6.

[46] S. M. Han, H. J. Lee, and J. Y. Choi, "Computer-aided prostate cancer detection using texture features and clinical features in ultrasound image," *J. Digit. Imag.*, vol. 21, no. 1, pp. 121–133, 2008.

[47] L. Hussain *et al.*, "Prostate cancer detection using machine learning techniques by employing combination of features extracting strategies," *Cancer Biomarkers*, vol. 21, no. 2, pp. 393–413, 2018.

[48] N. Friedman, M. Linial, I. Nachman, and D. Pe'er, "Using Bayesian networks to analyze expression data," *J. Comput. Biol.*, vol. 7, nos. 3–4, pp. 601–620, 2000.

[49] M. Sperrin and M. T. Lawton, "Multivariable and Bayesian network analysis of outcome predictors in acute aneurysmal subarachnoid hemorrhage: Review of a pure surgical series in the post-international subarachnoid aneurysm trial era," *Oper. Neurosurg.*, vol. 14, no. 6, pp. 603–610, 2018.

[50] Y. LeCun, Y. Bengio, and G. Hinton, "Deep learning," *Nature*, vol. 521, no. 7553, p. 436, 2015.

[51] J. Wang, X. Yang, H. Cai, W. Tan, C. Jin, and L. Li, "Discrimination of breast cancer with microcalcifications on mammography by deep learning," *Sci. Rep.*, vol. 6, p. 27327, Jun. 2016.

[52] V. Naranjo, R. Lloréns, M. Alcañiz, and F. López-Mir, "Metal artifact reduction in dental CT images using polar mathematical morphology," *Comput. Methods Programs Biomed.*, vol. 102, no. 1, pp. 64–74, 2011.

[53] M. Masseroli, A. Bollea, and G. Forloni, "Quantitative morphology and shape classification of neurons by computerized image analysis," *Comput. Methods Programs Biomed.*, vol. 41, no. 2, pp. 89–99, 1993.

[54] D. Welfer, J. Scharcanski, and D. R. Marinho, "Fovea center detection based on the retina anatomy and mathematical morphology," *Comput. Methods Programs Biomed.*, vol. 104, no. 3, pp. 397–409, 2011.

[55] S. Rathore, M. Hussain, M. A. Iftikhar, and A. Jalil, "Ensemble classification of colon biopsy images based on information rich hybrid features," *Comput. Biol. Med.*, vol. 47, no. 1, pp. 76–92, 2014.

[56] S. Rathore, A. Iftikhar, A. Ali, M. Hussain, and A. Jalil, "Capture largest included circles: An approach for counting red blood cells," in *Communications in Computer and Information Science*, vol. 281. Berlin, Germany: Springer, 2012, pp. 373–384.

[57] L. Hussain *et al.*, "A radial base neural network approach for emotion recognition in human speech," *Int. J. Comput. Sci. Netw. Secur.*, vol. 17, no. 8, pp. 52–62, 2017.

[58] L. Hussain, W. Aziz, Z. H. Kazmi, and I. A. Awan, "Classification of human faces and non faces using machine learning techniques," *Int. J. Electron. Electr. Eng.*, vol. 2, no. 2, pp. 116–123, Jun. 2014.

[59] L. Hussain, W. Aziz, S. A. Nadeem, and A. Q. Abbasi, "Classification of normal and pathological heart signal variability using machine learning techniques classification of normal and pathological heart signal variability using machine learning techniques," *Int. J. Darshan Inst. Eng. Res. Emerg. Technol.*, vol. 3, no. 2, pp. 13–19, 2015.

[60] L. Hussain, W. Aziz, A. S. Khan, A. Q. Abbasi, and S. Z. Hassan, "Classification of electroencephlography (EEG) alcoholic and control subjects using machine learning ensemble methods," *J. Multidiscip. Eng. Sci. Technol.*, vol. 2, no. 1, pp. 126–131, 2015.

[61] F. Khalvati, J. Zhang, A. G. Chung, M. J. Shafiee, A. Wong, and M. A. Haider, "MPCaD: A multi-scale radiomics-driven framework for automated prostate cancer localization and detection," *BMC Med. Imag.*, vol. 18, no. 1, p. 16, Dec. 2018.

[62] V. Fetz, H. Prochnow, M. Brönstrup, and F. Sasse, "Target identification by image analysis," *Natural Product Rep.*, vol. 33, no. 5, pp. 655–667, 2016.

[63] M. M. Usaj, E. B. Styles, A. J. Verster, H. Friesen, C. Boone, and B. J. Andrews, "High-content screening for quantitative cell biology," *Trends Cell Biol.*, vol. 26, no. 8, pp. 598–611, Aug. 2016.

[64] M. Boutros, F. Heigwer, and C. Laufer, "Microscopy-based high-content screening," *Cell*, vol. 163, no. 6, pp. 1314–1325, Dec. 2015.

[65] T. Kadir and F. Gleeson, "Lung cancer prediction using machine learning and advanced imaging techniques," *Transl. Lung Cancer Res.*, vol. 7, no. 3, pp. 304–312, 2018.

[66] K.-H. Yu *et al.*, "Predicting non-small cell lung cancer prognosis by fully automated microscopic pathology image features," *Nature Commun.*, vol. 7, p. 12474, Aug. 2016.

[67] X. Luo *et al.*, "Comprehensive computational pathological image analysis predicts lung cancer prognosis," *J. Thoracic Oncol.*, vol. 12, no. 3, pp. 501–509, Mar. 2017.

[68] H. Wang, F. Xing, H. Su, A. Stromberg, and L. Yang, "Novel image markers for non-small cell lung cancer classification and survival prediction," *BMC Bioinform.*, vol. 15, no. 1, p. 310, 2014.

[69] C. Isaza, K. Anaya, J. Z. de Paz, J. F. Vasco-Leal, I. Hernandez-Rios, and J. D. Mosquera-Artamonov, "Image analysis and data mining techniques for classification of morphological and color features for seeds of the wild castor oil plant *(Ricinus communis L.)*," *Multimed. Tools Appl.*, vol. 77, no. 2, pp. 2593–2610, Jan. 2018.

[70] D. G. Fatouros *et al.*, "Structural development of self Nano emulsifying drug delivery systems (SNEDDS) during *in vitro* lipid digestion monitored by small-angle X-ray scattering," *Pharm. Res.*, vol. 24, no. 10, pp. 1844–1853, Aug. 2007.

[71] M. R. Jahanshahi and S. F. Masri, "Adaptive vision-based crack detection using 3D scene reconstruction for condition assessment of structures," *Autom. Construct.*, vol. 22, pp. 567–576, Mar. 2012.

[72] T. Merazi-Meksen, M. Boudraa, and B. Boudraa, "Mathematical morphology for TOFD image analysis and automatic crack detection," *Ultrasonics*, vol. 54, no. 6, pp. 1642–1648, Aug. 2014.

[73] S. K. Sinha and P. W. Fieguth, "Automated detection of cracks in buried concrete pipe images," *Autom. Construct.*, vol. 15, no. 1, pp. 58–72, Jan. 2006.

[74] P. Broberg, "Surface crack detection in welds using thermography," *NDT & E Int.*, vol. 57, pp. 69–73, Jul. 2013.

[75] P. Wang and H. Huang, "Comparison analysis on present image-based crack detection methods in concrete structures," in *Proc. 3rd Int. Congr. Image Signal Process.*, 2010, pp. 2530–2533.

[76] S. Ibrahim *et al.*, "Classification of diabetes maculopathy images using data-adaptive neuro-fuzzy inference classifier," *Med. Biol. Eng. Comput.*, vol. 53, no. 12, pp. 1345–1360, Dec. 2015.

[77] A. M. Naguib, A. M. Ghanem, and A. S. Fahmy, "Content based image retrieval of diabetic macular edema images," in *Proc. 26th IEEE Int. Symp. Comput.-Based Med. Syst.*, Jun. 2013, pp. 560–562.

[78] C. G. Baby and D. A. Chandy, "Content-based retinal image retrieval using dual-tree complex wavelet transform," in *Proc. Int. Conf. Signal Process. Image Process., Pattern Recognit.*, 2013, pp. 195–199.

[79] P. Chowriappa, S. Dua, U. R. Acharya, and M. M. R. Krishnan, "Ensemble selection for feature-based classification of diabetic maculopathy images," *Comput. Biol. Med.*, vol. 43, no. 12, pp. 2156–2162, Dec. 2013.

[80] K. S. Deepak and J. Sivaswamy, "Automatic assessment of macular edema from color retinal images," *IEEE Trans. Med. Imag.*, vol. 31, no. 3, pp. 766–776, Mar. 2012.

[81] M. R. K. Mookiah *et al.*, "Application of higher-order spectra for automated grading of diabetic maculopathy," *Med. Biol. Eng. Comput.*, vol. 53, no. 12, pp. 1319–1331, Dec. 2015.

[82] A. Hunter, J. A. Lowell, B. Ryder, A. Basu, and D. Steel, "Automated diagnosis of referable maculopathy in diabetic retinopathy screening," in *Proc. Annu. Int. Conf. IEEE Eng. Med. Biol. Soc.*, Sep. 2011, pp. 3375–3378.

[83] H. Xu, C. Lu, R. Berendt, N. Jha, and M. Mandal, "Automated analysis and classification of melanocytic tumor on skin whole slide images," *Comput. Med. Imag. Graph.*, vol. 66, pp. 124–134, Jun. 2018.

[84] Y. M. Li and X. P. Zeng, "A new strategy for urinary sediment segmentation based on wavelet, morphology and combination method," *Comput. Methods Programs Biomed.*, vol. 84, nos. 2–3, pp. 162–173, 2006.

[85] G. Ertaş, H. Ö. Gülçür, E. Aribal, and A. Semiz, "Feature extraction from mammographic mass shapes and development of a mammogram database," *Annu. Rep. Res. React. Inst., Kyoto Univ.*, vol. 3, pp. 2752–2755, Oct. 2001.

[86] B. Surendiran and A. Vadivel, "Mammogram mass classification using various geometric shape and margin features for early detection of breast cancer," *Int. J. Med. Eng. Inform.*, vol. 4, no. 1, pp. 36–54, 2012.

[87] X. Bresson and T. F. Chan, "Fast dual minimization of the vectorial total variation norm and applications to color image processing," *Inverse Problems Imag.*, vol. 2, no. no. 4, pp. 455–484, 2008.

[88] J. Pearl, "Fusion, propagation, and structuring in belief networks," *Artif. Intell.*, vol. 29, no. 3, pp. 241–288, 1986.

[89] S. C. Bayesia, "BayesiaLab7," Bayesia, Lockhart Court Franklin, TN, USA, Tech. Rep. V18, 2017.

[90] C. E. Shannon, "A mathematical theory of communication," *Bell Syst. Tech. J.*, vol. 27, no. 3, pp. 379–423, Jul./Oct. 1948.

[91] S. Conrady and L. Jouffe, *Bayesian Networks and BayesiaLab: A Practical Introduction for Researchers*. Lockhart Court Franklin, TN, USA: Bayesia, 2015.

[92] X. Zhang *et al.*, "Inferring gene regulatory networks from gene expression data by path consistency algorithm based on conditional mutual information," *Bioinformatics*, vol. 28, no. 1, pp. 98–104, 2012.

[93] X. Zhang, J. Zhao, J.-K. Hao, X.-M. Zhao, and L. Chen, "Conditional Mutual inclusive information enables accurate quantification of associations in gene regulatory networks," *Nucleic Acids Res.*, vol. 43, no. 5, p. e31, 2015.

[94] F. Xiao, L. Gao, Y. Ye, Y. Hu, and R. He, "Inferring gene regulatory networks using conditional regulation pattern to guide candidate genes," *PLoS ONE*, vol. 11, no. 5, pp. 1–13, 2016.

[95] D. Janzing, D. Balduzzi, M. Grosse-Wentrup, and B. Schölkopf, "Quantifying causal influences," *Ann. Statist.*, vol. 41, no. 5, pp. 2324–2358, 2013.

[96] J. L. Rodgers and W. A. Nicewander, "Thirteen ways to look at the correlation coefficient," *Amer. Statist.*, vol. 42, no. 1, pp. 59–66, 1988.

[97] S. K. Tyagi, "Correlation coefficient of dual hesitant fuzzy sets and its applications," *Appl. Math. Model.*, vol. 39, no. 22, pp. 7082–7092, 2015.

[98] H. Liao, Z. Xu, and X.-J. Zeng, "Novel correlation coefficients between hesitant fuzzy sets and their application in decision making," *Knowl.-Based Syst.*, vol. 82, pp. 115–127, Jul. 2015.

[99] M.-T. Puth, M. Neuhäuser, and G. D. Ruxton, "Effective use of Pearson's product–moment correlation coefficient," *Animal Behav.*, vol. 93, pp. 183–189, Jul. 2014.

[100] Y. Kim, T.-H. Kim, and T. Ergün, "The instability of the Pearson correlation coefficient in the presence of coincidental outliers," *Finance Res. Lett.*, vol. 13, pp. 243–257, May 2015.

[101] D. Barber, *Bayesian Reasoning and Machine Learning*. Cambridge, U.K.: Cambridge Univ. Press, 2012.

[102] D. C. Thomas, D. V. Conti, J. Baurley, F. Nijhout, M. Reed, and C. M. Ulrich, "Use of pathway information in molecular epidemiology," *Hum. Genomics*, vol. 4, no. 1, pp. 21–42, 2009.

[103] C. Su, A. Andrew, M. R. Karagas, and M. E. Borsuk, "Using Bayesian networks to discover relations between genes, environment, and disease," *BioData Min.*, vol. 6, no. 1, pp. 1–21, 2013.

[104] R. Myte, B. Gylling, J. Häggström, J. Schneede, and P. M. Ueland, "Untangling the role of one-carbon metabolism in colorectal cancer risk: A comprehensive Bayesian network analysis," *Sci. Rep.*, vol. 7, Oct. 2017, Art. no. 43434.

[105] M. G. Kendall, "A new measure of rank correlation," *Biometrika*, vol. 30, nos. 1–2, pp. 81–93, Jun. 1938.

[106] C. Spearman, "'General intelligence'objectively determined and measured," *Amer. J. Psychol.*, vol. 15, no. 2, pp. 201–294, Apr. 1904.

[107] C. Reimann, P. Filzmoser, K. Hron, P. Kynčlová, and R. G. Garrett, "A new method for correlation analysis of compositional (environmental) data—A worked example," *Sci. Total Environ.*, vols. 607–608, pp. 965–971, Dec. 2017.

[108] J. Pearl and T. S. Verma, "A theory of inferred causation," *Stud. Logic Found. Math.*, vol. 134, pp. 789–811, Apr. 1995.

[109] D. Heckerman, C. Meek, and G. Cooper, "A Bayesian approach to causal discovery," in *Innovations in Machine Learning*. Berlin, Germany: Springer-Verlag, 2006, pp. 1–28.

[110] T. Burr, "Causation, prediction, and search," *Technometrics*, vol. 45, no. 3, pp. 272–273, Aug. 2003.

[111] S.-T. Liu and C. Kao, "Fuzzy measures for correlation coefficient of fuzzy numbers," *Fuzzy Sets Syst.*, vol. 128, no. 2, pp. 267–275, Jun. 2002.

[112] C. Yu, "Correlation of fuzzy numbers," *Fuzzy Sets Syst.*, vol. 55, no. 3, pp. 303–307, May 1993.

[113] D.-A. Chiang and N. P. Lin, "Correlation of fuzzy sets," *Fuzzy Sets Syst.*, vol. 102, no. 2, pp. 221–226, Mar. 1999.

[114] B. B. Chaudhuri and A. Bhattacharya, "On correlation between two fuzzy sets," *Fuzzy Sets Syst.*, vol. 118, no. 3, pp. 447–456, 2001.

[115] C. A. Murthy, S. K. Pal, and D. D. Majumder, "Correlation between two fuzzy membership functions," *Fuzzy Sets Syst.*, vol. 17, no. 1, pp. 23–38, Sep. 1985.

[116] Z. Xu and M. Xia, "On distance and correlation measures of hesitant fuzzy information," *Int. J. Intell. Syst.*, vol. 26, no. 5, pp. 410–425, May 2011.

[117] N. Chen, Z. Xu, and M. Xia, "Correlation coefficients of hesitant fuzzy sets and their applications to clustering analysis," *Appl. Math. Model.*, vol. 37, no. 4, pp. 2197–2211, Feb. 2013.

[118] Z. Xu, "On correlation measures of intuitionistic fuzzy sets," in *Proc. Int. Conf. Intell. Data Eng. Automated Learn.*, 2006, pp. 16–24.

[119] W.-L. Hung and J.-W. Wu, "Correlation of intuitionistic fuzzy sets by centroid method," *Inf. Sci.*, vol. 144, nos. 1–4, pp. 219–225, Jul. 2002.

[120] D. H. Hong and S. Y. Hwang, "Correlation of intuitionistic fuzzy sets in probability spaces," *Fuzzy Sets Syst.*, vol. 75, no. 1, pp. 77–81, Oct. 1995.

[121] H. B. Mitchell, "A correlation coefficient for intuitionistic fuzzy sets," *Int. J. Intell. Syst.*, vol. 19, no. 5, pp. 483–490, May 2004.

[122] T. Gerstenkorn and J. Mańko, "Correlation of intuitionistic fuzzy sets," *Fuzzy Sets Syst.*, vol. 44, no. 1, pp. 39–43, Nov. 1991.

[123] W.-L. Hung, "Using statistical viewpoint in developing correlation of intuitionistic fuzzy sets," *Int. J. Uncertainty, Fuzziness Knowl.-Based Syst.*, vol. 9, no. 4, pp. 509–516, Aug. 2001.

[124] J.-P. Onnela, K. Kaski, and J. Kertész, "Clustering and information in correlation based financial networks," *Eur. Phys. J. B*, vol. 38, no. 2, pp. 353–362, 2004.

[125] F. L. da Silva, J. P. Pijn, and P. Boeijinga, "Interdependence of EEG signals: Linear vs. nonlinear associations and the significance of time delays and phase shifts," *Brain Topogr.*, vol. 2, nos. 1–2, pp. 9–18, 1989.

[126] A. Hyvärinen and E. Oja, "Independent component analysis: Algorithms and applications," *Neural Netw.*, vol. 13, nos. 4–5, pp. 411–430, Jun. 2000.

[127] A. F. Villaverde, J. Ross, F. Morán, and J. R. Banga, "MIDER: Network inference with mutual information distance and entropy reduction," *PLoS ONE*, vol. 9, no. 5, p. e96732, May 2014.
[128] R. Steuer, J. Kurths, C. O. Daub, J. Weise, and J. Selbig, "The mutual information: Detecting and evaluating dependencies between variables," *Bioinformatics*, vol. 18, no. 2, pp. S231–S240, Oct. 2002.
[129] Y. X. Wang and H. Huang, "Review on statistical methods for gene network reconstruction using expression data," *J. Theor. Biol.*, vol. 362, pp. 53–61, Dec. 2014.
[130] C. O. Daub, R. Steuer, J. Selbig, and S. Kloska, "Estimating mutual information using B-spline functions—An improved similarity measure for analysing gene expression data," *BMC Bioinformat.*, vol. 5, no. 1, p. 118, 2004.
[131] A. Kraskov, H. Stögbauer, and P. Grassberger, "Estimating mutual information," *Phys. Rev. E*, vol. 69, p. 066138, Jun. 2004.
[132] J. P. W. Pluim, J. B. A. Maintz, and M. A. Viergever, "Mutual-information-based registration of medical images: A survey," *IEEE Trans. Med. Imag.*, vol. 22, no. 8, pp. 986–1004, Aug. 2003.

**LAL HUSSAIN** received the M.S. degree in communication and networks from Iqra University, Islamabad, Pakistan, in 2012, with Gold medal, and the Ph.D. degree from the Department of Computer Science and Information Technology, University of Azad Jammu and Kashmir, Muzaffarabad, Pakistan, in 2016. He is currently a Programmer with the Department of Computer Science and IT, University of Azad Jammu and Kashmir. He was a Visiting Ph.D. Researcher with Lancaster University, U.K., for six months, under the HEC International Research Initiative Program and worked under the supervision of Dr. A. Stefanovska, and a Professor of biomedical physics with the Physics Department, Lancaster University. He has authored more than 20 publications in highly reputed peer reviewed and Impact Fact Journals. He presented various talks in Pakistan, U.K., and USA. His research interests include biomedical signal processing with concentration in complexity measures, time-frequency representation methods, and cross frequency coupling to analyze the dynamics of neurophysiological and physiological signals. His research interests also include neural networks and machine learning classification, regression and prediction techniques for detection of cancer, epilepsy, brain dynamics and diseases (i.e., autism spectrum disorder and attention-deficit/hyperactivity disorder, Alzheimer's disease, brain tumor), image processing, and segmentation.

**AMJAD ALI** received the B.S. and M.S. degrees in computer science from the COMSATS Institute of Information Technology, Pakistan, in 2006 and 2008, respectively, and the Ph.D. degree from the Electronics and Radio Engineering Department, Kyung Hee University, South Korea, in 2015. He is currently a Post-Doctoral Fellow with the Mobile Network and Communication Lab, School of Electrical Engineering, Korea University, Anam-dong, Seoul, South Korea. Since 2015, he has been an Assistant Professor with the Department of Computer Science, COMSATS University Islamabad, Lahore Campus. His main research interests include the Internet of Things, cognitive radio networks (interference modeling, dynamic spectrum access, power and admission control, spectrum management, spectrum trading, MAC protocols, performance modeling, and optimization), 5G cellular networks (spectrum/resource management, coexistence, distributed wireless access, scheduling, power control, network selection, mobility/handover management), multimedia processing, machine learning, hoc social networks, multimedia cloud computing, smart grid, and vehicular networks.

**SAIMA RATHORE** received the B.S. degree in software engineering from Fatima Jinnah Women University, Rawalpindi, Pakistan, in 2006, and the M.S. degree in computer engineering from the University of Engineering and Technology, Taxila, Pakistan, in 2008, and the Ph.D. degree in computer science from the Pakistan Institute of Engineering and Applied Sciences, Islamabad, Pakistan, in 2015. She is currently a Post-Doctoral Researcher with the Perelman School of Medicine, University of Pennsylvania, USA. Her research interests include computer-aided medical diagnosis.

**SHARJIL SAEED** received the master's degree in computer system engineering from the GIK Institute, Swabi Technology, University of Azad Jammu and Kashmir, and the Ph.D. degree from the University of Azad Jammu and Kashmir, in 2016. He has a vast teaching and research experience. He is currently the Chairman at the Department of Computer Science and Information. He has published several journal and conference articles. His research interests include biomedical signal processing, machine learning, quantification and non-linear analysis.

**ADNAN IDRIS** received the master's degree in software engineering from the COMSTATS Institute of IT, Islamabad, in 2002, the M.S. degree in computer system engineering from the GIK Institute of Engineering Sciences and Technology Topi, Pakistan, in 2006, and the Ph.D. degree from the Pakistan Institute of Engineering and Applied Sciences, Islamabad, in 2015. Further, he has more than 15 years of research and teaching experience at university level. He is currently an Assistant Professor with the Department of Computer Sciences and IT, The University of Poonch Rawalakot. His research areas include customer churn prediction, bio-informatics machine learning, pattern recognition and evolutionary algorithms.

**MUHAMMAD USAMA USMAN** received the B.Sc. degree in electrical and electronics engineering from the University of Engineering and Technology, Pakistan, in 2008, and the M.Sc. degree in electrical engineering from Florida State University, USA, in 2014, where he is currently pursuing the Ph.D. degree with the Department of Electrical and Computer Engineering. He was a Lecturer with the Department of Electrical Engineering, UAJK, from 2014 to 2015. He also has over four years of industrial experience as an Electrical Engineer. He is also a Graduate Research Assistant at the Center for Advanced Power Systems. His research interests include all aspects of smart grids and machine learning.

**MUHAMMAD AKSAM IFTIKHAR** received the B.S. degree in computer engineering and the M.S. degree in computer science from the University of Engineering and Technology, Lahore, in 2007 and 2010, respectively, and the Ph.D. degree from the Pakistan Institute of Engineering and Applied Sciences, Islamabad, in 2014. He has more than seven years of professional and teaching/research experience to his credit. He has published 12 research articles in Impact Factor journals (ISI-indexed) of international repute and has presented 15 research papers in international IEEE/Springer conferences. His primary research areas include image processing (especially medical image processing and analysis), computer vision, and pattern recognition. His personal interests include book reading, outdoor sports (especially swimming and martial arts), and hiking.

**DOUG YOUNG SUH** (S'89–M'90) received the B.S. degree in nuclear engineering from Seoul National University, Seoul, South Korea, in 1980, and the Ph.D. degree in electrical and computer engineering from the Georgia Institute of Technology, Atlanta, GA, USA, in 1990. In 1990, he joined the Korea Academy of Industry and Technology and conducted research on HDTV, until 1992. Since 1992, he has been a Professor with the College of Electronics and Information, Kyung Hee University, Seoul, South Korea. He has been a Korean delegate for the ISO/IEC MPEG Forum, since 1996. His research interests include networked video and computer game.